Chaotic Mixer for Microchannels

Abraham D. Stroock,[1]* Stephan K. W. Dertinger,[1] Armand Ajdari,[2] Igor Mezić,[3] Howard A. Stone,[4] George M. Whitesides[1]*

It is difficult to mix solutions in microchannels. Under typical operating conditions, flows in these channels are laminar—the spontaneous fluctuations of velocity that tend to homogenize fluids in turbulent flows are absent, and molecular diffusion across the channels is slow. We present a passive method for mixing streams of steady pressure-driven flows in microchannels at low Reynolds number. Using this method, the length of the channel required for mixing grows only logarithmically with the Péclet number, and hydrodynamic dispersion along the channel is reduced relative to that in a simple, smooth channel. This method uses bas-relief structures on the floor of the channel that are easily fabricated with commonly used methods of planar lithography.

Microfluidic systems are now widely used in biology and biotechnology; applications include analysis (of DNA and proteins) (*1*), sorting (of cells) (*2*), high-throughput screening (*3*), chemical reactions (*4*), and transfers of small volumes (1 to 100 nl) of materials (*5*). Typical uses of microfluidic devices (e.g., chemical analysis in the field) require that these systems be inexpensive and simple to operate; microfluidic components that operate with pressure flow and few moving parts are desirable. Microfluidic designs should also be compatible with the planar, layer-by-layer geometries that are imposed by current, lithography-based techniques of microfabrication. Physically, flows of common liquids at practical pressures in microfluidic channels (typical cross-sectional dimension, $l \sim 100$ μm) are characterized by low values of the Reynolds number ($Re = Ul/\nu < 100$, where U is the average flow speed and ν is the kinematic viscosity of the fluid) (*6*); general strategies for controlling flow in microfluidic devices should not depend on inertial effects, because these only become important for $Re \gg 1$.

Mixing of the fluid flowing through microchannels is important in a variety of applications: e.g., in the homogenization of solutions of reagents used in chemical reactions, and in the control of dispersion of material along the direction of Poiseuille flows (*7*, *8*). At low *Re*, in simple channels (i.e., with smooth walls), pressure flows are laminar and uniaxial, so the mixing of material between streams in the flow is purely diffusive. Even on the scale of a microchannel, this diffusive mixing is slow compared with the convection of material along the channel; the Péclet number is large ($Pe = Ul/D > 100$, where D is the molecular diffusivity) (*9*). For such uniaxial flows, the distance along the channel that is required for mixing to occur is $\Delta y_m \sim U \times (l^2/D) = Pe \times l$ (*10*). This mixing length can be prohibitively long ($\gg$1 cm) and grows linearly with *Pe*.

To reduce the mixing length there must be transverse components of flow that stretch and fold volumes of fluid over the cross section of the channel. These stirring flows will reduce the mixing length by decreasing the average distance, Δr, over which diffusion must act in the transverse direction to homogenize unmixed volumes. In a steady chaotic flow, the stretching and folding of volumes of the fluid proceed exponentially as a function of the axial distance traveled by the volume: $\Delta r = l \exp(-\Delta y/\lambda)$, where the initial transverse distance is taken to be l, and λ is a characteristic length determined by the geometry of trajectories in the chaotic flow (*11*, *12*). For large *Pe*, in a flow that is chaotic over most of its cross section, we expect an important reduction of the mixing length relative to that in an unstirred flow: $\Delta y_m \sim \lambda \ln(Pe)$ (*13*).

Several protocols for mixing based on chaotic flows have been proposed and demonstrated in macroscopic systems (typical dimension >1 cm) (*12*); mixing on microscales remains difficult. The group of Beebe has demonstrated chaotic stirring in a helical microchannel; in this design, stirring occurs as a result of eddies at the bends in the channel in flows of intermediate *Re* (i.e., $Re > 1$) (*14*). This mixer is complicated to fabricate and inefficient at low *Re* ($Re < 1$). Active mixers require either external, variable-frequency pumps or internal moving components (*15*). Active mixers require variable-frequency pumps off-chip or moving components on-chip. Here, we present a general strategy for creating transverse flows in microchannels that can be used to induce chaotic stirring at low *Re* ($0 < Re < 100$).

To generate transverse flows in microchannels by using a steady axial pressure gradient, we place ridges on the floor of the channel at an oblique angle, θ, with respect to the long axis ($\hat{y}$) of the channel (Fig. 1A). This type of structure can be fabricated with two steps of photolithography. We used soft lithographic methods to make the channels in poly(dimethylsiloxane) (*16*, *17*). These ridges—similar to rifling in a gun barrel—present an anisotropic resistance to viscous flows (flows with low *Re*): There is less resistance to flow in the direction parallel to the peaks and valleys of the ridges (along $\hat{y}'$) than in the orthogonal direction (along $\hat{x}'$) (*18*). As a result of this anisotropy, an axial pressure gradient (along $\hat{y}$) generates a mean (averaged over a period of the topography) transverse component in the flow (along $\hat{x}$) that originates at the structured surface; the fluid circulates back across the top of the channel (along $-\hat{x}$). As indicated schematically by the two trajectories drawn in Fig. 1A, the full flow has helical streamlines. The optical micrograph in Fig. 1B shows the trajectories of two streams of fluid (red and green) in a microchannel such as the one in Fig. 1A.

The frames in Fig. 1C are confocal micrographs of the vertical cross section of a channel similar to those in Fig. 1, A and B. As indicated on these images, we use the leading edge of the fluorescent region to measure the angular displacement of the fluid in the cross section, $\Delta\phi$. Within the Stokes flow regime ($Re < 1$) and for small ridges relative to the height of the channel (relative height, $\alpha < 0.3$), we have checked that the form of the flow (i.e., the shape of the trajectories) is independent of *Re*. We also found that the form of the flow remains qualitatively the same for $Re < 100$. Furthermore, the experimentally observed dependence of the average rate of rotation, $d\Delta\phi/dy$, on geometrical parameters (q, h, w, and θ) can be rationalized with a simple model (*19*, *20*).

The ability to generate transverse flows in microchannels makes it possible to de-

[1]Department of Chemistry and Chemical Biology, Harvard University, Cambridge, MA 02138, USA. [2]Laboratoire de Physico-Chimie Théorique, CNRS UMR 7083, École Supérieure de Physique et de Chimie Industrielles de la Ville de Paris, Paris, France. [3]Department of Mechanical and Environmental Engineering and Department of Mathematics, University of California, Santa Barbara, CA 93106, USA. [4]Division of Engineering and Applied Sciences, Harvard University, Cambridge, MA 02138, USA.

*To whom correspondence should be addressed. E-mail: stroock@fas.harvard.edu, gwhitesides@gmwgroup.harvard.edu

sign steady chaotic flows for use in microfluidic systems. A mixer based on patterns of grooves on the floor of the channel is shown schematically in Fig. 2A; we refer to this design as the staggered herringbone mixer (SHM). One way to produce a chaotic flow is to subject volumes of fluid to a repeated sequence of rotational and extensional local flows (*21*). This sequence of local flows is achieved in the SHM by varying the shape of the grooves as a function of axial position in the channel: The change in the orientation of the herringbones between half cycles exchanges the positions of the centers of rotation (local rotational flow, "c" in the Fig. 2A) and the up- and down-wellings (local extensional flow, "u" and "d" in Fig. 2A) in the transverse flow. Figure 2B shows the evolution of two streams through one cycle of the SHM.

In the SHM, the efficiency of mixing is controlled by two parameters: p, a measure of the asymmetry of the herringbones; and $\Delta\phi_m$, a measure of the amplitude of the rotation of the fluid in each half cycle (*22*). The angular displacement, $\Delta\phi_m$, is controlled by the geometry of the ridges (*20*) and the number of herringbones per half cycle (10 in the case shown in Fig. 2). As p goes to one-half (i.e., symmetric herringbones) or $\Delta\phi_m$ goes to zero, the flow becomes nonchaotic. For $p = 2/3$ and $\Delta\phi_m > 60°$, most of the cross-sectional area is involved in the chaotic flow (*23*). As in the twisting flow (Fig. 1), the form of flow in the SHM is independent of *Re* in the Stokes regime, and we have verified experimentally that it remains qualitatively the same for $Re < 100$.

The diagrams in Fig. 3, A to C, show the experiments we used to characterize mixing. At the entrance of the channel, distinct streams of a fluorescent and a clear solution fill opposite halves of the cross section of the channel. The micrographs in Fig. 3, A and B, show that for flows with high Péclet number ($Pe = 2 \times 10^5$), there is negligible mixing in a simple channel (Fig. 3A) and incomplete mixing in a channel with straight ridges (Fig. 3B) after the flow has proceeded 3 cm—the typical dimension of a microfluidic chip—down the channel. The confocal cross sections in Fig. 3C show that thorough mixing occurs at even higher Pe (9×10^5) in a channel that contains the SHM (*24*). The micrographs in Fig. 3C also show the rapid increase in the number of filaments and decrease in their thickness, Δr, as a function of the number of mixing cycles.

To quantify the degree of mixing (convection plus diffusion) as a function of the axial distance traveled in the mixer and of *Pe*, we measure the standard deviation of the intensity distribution in confocal images of the cross section of the flow like those in Fig. 3, A to C: $\sigma = \langle (I - \langle I \rangle)^2 \rangle^{1/2}$, where I is the grayscale value (between 0 and 1) of a pixel, and $\langle\ \rangle$ means an average over all the pixels in the image. The value of σ is

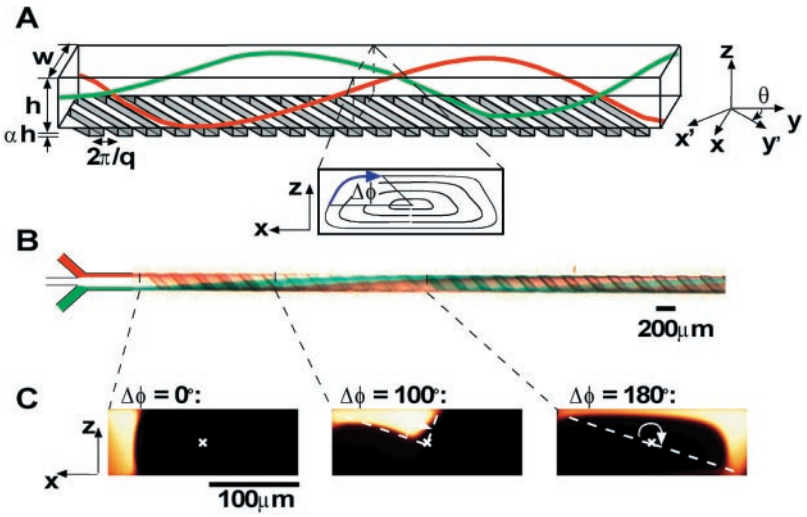

Fig. 1. Three-dimensional twisting flow in a channel with obliquely oriented ridges on one wall. (**A**) Schematic diagram of channel with ridges. The coordinate systems (x, y, z) and (x', y', z) define the principal axes of the channel and of the ridges. The angle θ defines the orientation of the ridges with respect to the channel. The amplitude of the ridges, αh, is small compared to the average height of the channel, h ($\alpha < 0.3$). The width of the channel is w and principal wavevector of the ridges is q. The red and green lines represent trajectories in the flow. The streamlines of the flow in the cross section are shown below the channel. The angular displacement, $\Delta\phi$, is evaluated on an outer streamline. (**B**) Optical micrograph showing a top view of a red stream and a green stream flowing on either side of a clear stream in a channel such as in (A) with $h = 70$ μm, $w = 200$ μm, $\alpha = 0.2$, $q = 2\pi/200$ μm^{-1}, and $\theta = 45°$. (**C**) Fluorescent confocal micrographs of vertical cross sections of a microchannel such as in (A). The frames show the rotation and distortion of a stream of fluorescent solution that was injected along one side of the channel such as the stream of green solution in (B). The measured values of $\Delta\phi$ are indicated (*29*).

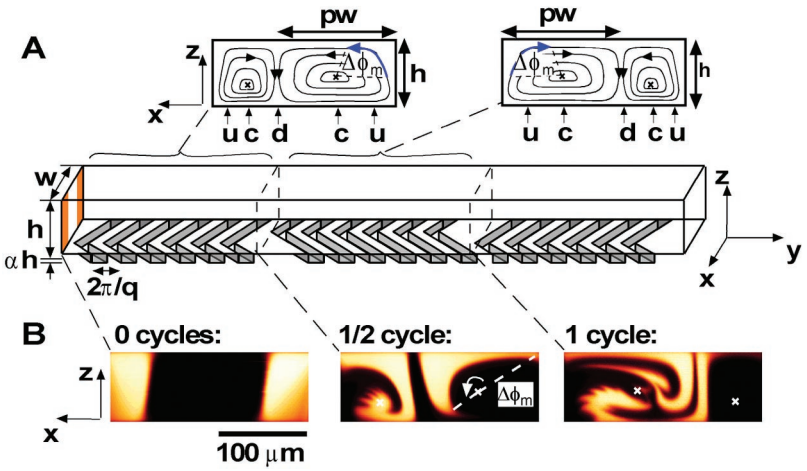

Fig. 2. Staggered herringbone mixer (SHM). (**A**) Schematic diagram of one-and-a-half cycles of the SHM. A mixing cycle is composed of two sequential regions of ridges; the direction of asymmetry of the herringbones switches with respect to the centerline of the channel from one region to the next. The streamlines of the flow in the cross section are shown schematically above the channel. The angle, $\Delta\phi_m$, is the average angular displacement of a volume of fluid along an outer streamline over one half cycle in the flow generated by the wide arms of the herringbones. The fraction of the width of the channel occupied by the wide arms of the herringbones is p. The horizontal positions of the centers of rotation, the upwellings, and the downwellings of the cellular flows are indicated by c, u, and d, respectively. (**B**) Confocal micrographs of vertical cross sections of a channel as in (A). Two streams of fluorescent solution were injected on either side of a stream of clear solution (*29*). The frames show the distribution of fluorescence upstream of the features, after one half cycle, and after one full cycle. The fingerlike structures at the end of the fluorescent filaments on the bottom left of the second two frames are due to the weak separation of streamlines that occurs in the rectangular grooves even at low *Re*. In this experiment, $h = 77$ μm, $w = 200$ μm, $\alpha = 0.23$, $q = 2\pi/100$ μm^{-1}, $p = 2/3$, and $\theta = 45°$, and there were 10 ridges per half cycle. $Re < 10^{-2}$. $\Delta\phi_m \sim 180°$.

0.5 for completely segregated streams and 0 for completely mixed streams. Figure 3D shows the evolution of σ for flows of different *Pe* in the SHM (open symbols), in a simple channel as in Fig. 3A (▲), and in a channel with straight ridges as in Fig. 3B (●). We see that the SHM performs well over a large range in *Pe*; as *Pe* increases by a factor of ~500 ($Pe = 2 \times 10^3$ to $Pe = 9 \times 10^5$), the mixing length, Δy_{90}, required for 90% mixing (dashed line), increases by less than a factor of 3 ($\Delta y_{90} = 0.7$ cm to $\Delta y_{90} = 1.7$ cm). In Fig. 3E, we see that Δy_{90} increases linearly with ln(*Pe*) for large *Pe*, as expected for chaotic flows. Within the limits of our simple model of mixing (*13*), we estimate from the linear portion of the plot in Fig. 3E that λ is on the order of a few millimeters; the average width of the filaments of unmixed fluid decreases by a factor of ~3 as the fluid travels this axial distance. This estimate agrees qualitatively with the evolution seen in Fig. 3C.

On the basis of the results presented in Fig. 3, consider mixing a stream of protein solution in aqueous buffer (molecular weight 10^5, $D \sim 10^{-6}$ cm^2/s) with $U = 1$ cm/s and $l = 0.01$ cm. For this system, $Pe = 10^4$. The mixing length in a simple microchannel would be $\Delta y_m \sim Pe \times l = 100$ cm. On the basis of Fig. 3D, the mixing length in the SHM would be, $\Delta y_m \sim 1$ cm. Furthermore, increasing the flow speed by a factor of 10 (i.e., to $Pe = 10^5$) will increase the mixing length in the SHM to $\Delta y_m \sim 1.5$ cm. With the same change in flow speed, the mixing length in the absence of stirring will increase 10-fold, to $\Delta y_m \sim 10^3$ cm.

An important application of mixing in pressure flows is in the reduction of axial dispersion. Axial dispersion is important in determining performance in pressure-driven chromatography—e.g., in the transfer of fractions from a separation column to a point detector—where it leads to peak broadening. The most rapid dispersion of a band of solute takes place when its axial length is much shorter than the mixing length of the solute in the flow. During this stage, the length of the band grows at the maximum speed of the flow (i.e., more quickly than the center of the band moves along the channel). This effect is illustrated schematically in the diagram in Fig. 4A for an unstirred Poiseuille flow. Once the length of the band is greater than the mixing length, volumes of fluid have sampled both fast and slow regions of the flow, and the broadening of the band becomes diffusive, i.e. $\sim \sqrt{D_{\text{eff}} \tau_r}$, where D_{eff} is an effective diffusivity that again depends on the mixing length and τ_r is the residence time of the band in the flow (*8*, *25*).

The experiments presented in Fig. 4 demonstrate that, by stirring the fluid in the cross section of the flow, the SHM (Fig. 4C) reduces the extent of the initial, rapid broadening of a band of material relative to that in an unstirred flow (Fig. 4B). The mixing length in the unstirred flow is $\Delta y_m \sim 100$ cm. In this case, the asymmetry of the trace of fluorescence intensity as a function of time measured near the end of the channel (green trace in Fig. 4B) indicates that the band is still broadening rapidly as it reaches the end of the channel: The fluorescent fluid in the fast, uniform flow near the center of the channel is weakly dispersed and arrives at the detector first (steep initial rise of the trace); the fluorescent fluid in the shear flow near the walls is strongly dispersed and arrives at the detector later (long tail of the trace). With the SHM (Fig. 4C), the mixing length is $\Delta y_m \sim 1$ cm (estimated from the curves in Fig. 3D for $Pe = 10^4$). In this case, the band broadens rapidly in the first few centimeters of the channel as indicated by the asymmetry of the trace acquired 2 cm downstream from the inlet (blue trace in Fig. 4C). The traces acquired further downstream are noticeably more symmetrical; this change in-

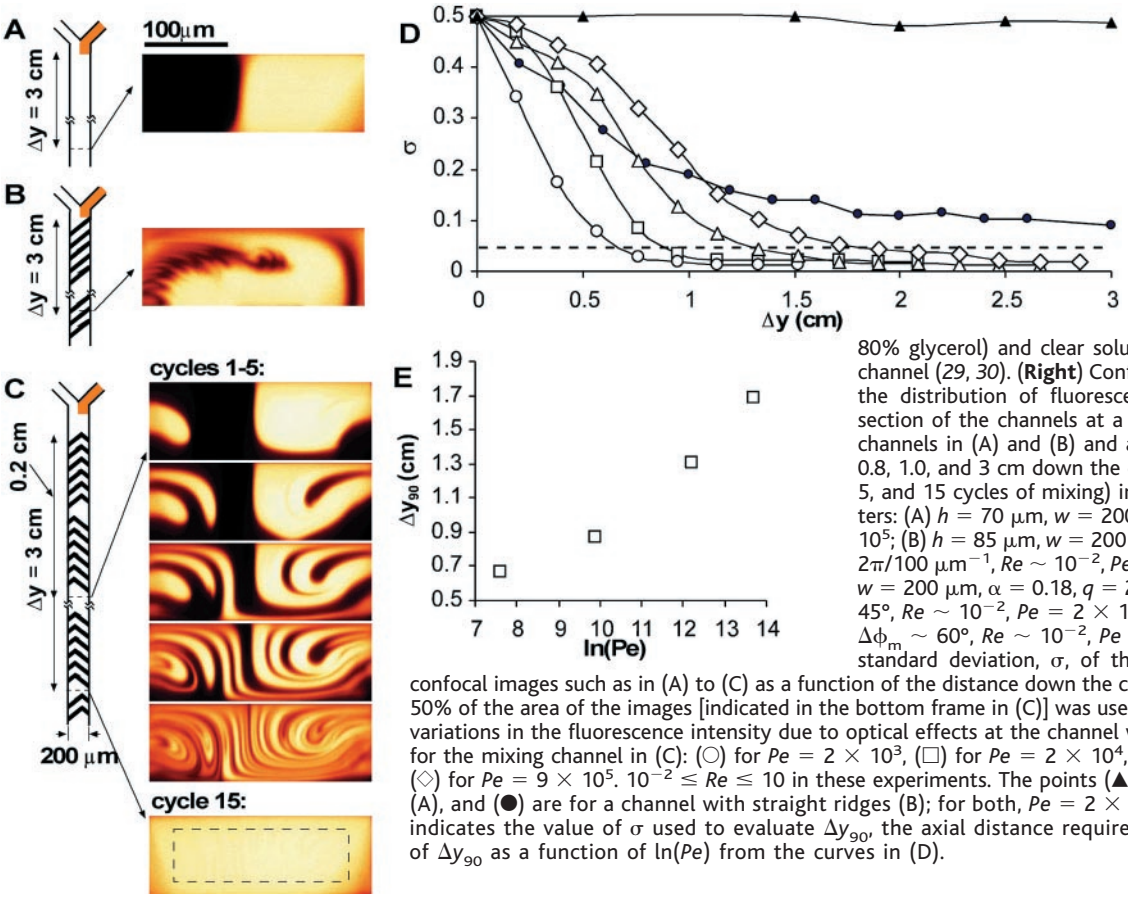

Fig. 3. Performance of SHM. (**A** to **C**) (**Left**) Schematic diagrams of channels with no structure on the walls (A), with straight ridges as in Fig. 1 (B), and with the staggered herringbone structure as in Fig. 2 (C). In each case, equal streams of a 1 mM solution of fluoroscein-labeled polymer in water/glycerol mixtures (0 and 80% glycerol) and clear solution were injected into the channel (*29*, *30*). (**Right**) Confocal micrographs that show the distribution of fluorescent molecules in the cross section of the channels at a distance of 3 cm down the channels in (A) and (B) and at distances of 0.2, 0.4, 0.6, 0.8, 1.0, and 3 cm down the channel (i.e., after 1, 2, 3, 4, 5, and 15 cycles of mixing) in (C). Experimental parameters: (A) $h = 70$ μm, $w = 200$ μm, $Re \sim 10^{-2}$, $Pe = 2 \times 10^5$; (B) $h = 85$ μm, $w = 200$ μm, $\alpha = 0.18$, $\theta = 45°$, $q = 2\pi/100$ μm^{-1}, $Re \sim 10^{-2}$, $Pe = 2 \times 10^5$; (C) $h = 85$ μm, $w = 200$ μm, $\alpha = 0.18$, $q = 2\pi/100$ μm^{-1}, $p = 2/3$, $\theta = 45°$, $Re \sim 10^{-2}$, $Pe = 2 \times 10^5$, six ridges per half-cycle, $\Delta\phi_m \sim 60°$, $Re \sim 10^{-2}$, $Pe = 9 \times 10^5$. (**D**) Plot of the standard deviation, σ, of the fluorescence intensity in confocal images such as in (A) to (C) as a function of the distance down the channel, Δ*y*. Only the central 50% of the area of the images [indicated in the bottom frame in (C)] was used to measure σ to eliminate variations in the fluorescence intensity due to optical effects at the channel walls. The open symbols are for the mixing channel in (C): (○) for $Pe = 2 \times 10^3$, (□) for $Pe = 2 \times 10^4$, (△) for $Pe = 2 \times 10^5$, and (◇) for $Pe = 9 \times 10^5$. $10^{-2} \leq Re \leq 10$ in these experiments. The points (▲) are for a smooth channel (A), and (●) are for a channel with straight ridges (B); for both, $Pe = 2 \times 10^5$. Horizontal dotted line indicates the value of σ used to evaluate Δy_{90}, the axial distance required for 90% mixing. (**E**) Plot of Δy_{90} as a function of ln(*Pe*) from the curves in (D).

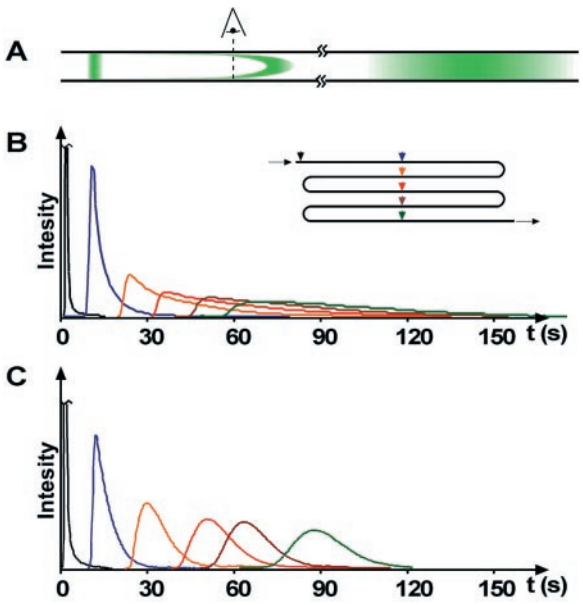

Fig. 4. Axial dispersion with and without SHM. (**A**) Schematic drawing illustrating the dispersion of a plug in Poiseuille flow. (**B**) Unstirred Poiseuille flow in a rectangular channel: $h = 70$ μm, $w = 200$ μm, and $Pe \sim 10^4$. (**C**) Stirred flow in a staggered herringbone mixer of the same design as in Fig. 3C; $Pe \sim 10^4$. In (B) and (C), a plug of fluorescent dye was introduced into serpentine channels of the form shown in the inset in (B). The traces represent the time evolution of the total fluorescence intensity (arbitrary units) as observed experimentally with a fluorescence microscope (2.5×/0.07 numerical aperture lens that averaged over the cross section of the channel) at different axial positions along the channel: 0 cm (black), 2.0 cm (blue), 6.2 cm (orange), 10.4 cm (red), 14.6 cm (brown), and 18.8 cm (green) downstream. The black traces (0 cm) have been truncated. The dye was fluorescein and the liquid was 80% glycerol/20% water. $D \sim 10^{-7}$ cm^2/s.

dicates a transition to diffusive broadening. Note that, by reducing the mixing length, the SHM will also reduce D_{eff} (*8*, *26*).

The SHM based on topography patterned on the inner surfaces of microchannels offers a general solution to the problem of mixing fluids in microfluidic systems. The simplicity of its design allows it to be integrated easily into microfluidic structures with standard microfabrication techniques. A single design will operate efficiently over a wide range of Re (we have observed good mixing for $0 < Re < 100$) and Pe (a SHM that is 3 cm long will fully mix all flows with $Pe < 10^6$). This design adds a negligible resistance to flow relative to that of a simple channel of the same dimensions. More generally, topography on the walls of microchannels can be used to manipulate the position of streams in a microchannel. For example, Fig. 1 demonstrates that two streams can cross over one another in a channel with only diffusional mixing.

We note that patterned topography on surfaces such as the staggered herringbone design can be used to generate chaotic flows in contexts other than pressure-driven flows in microchannels. For example, similar structures on the walls of round pipes and capillaries will generate efficient mixing flows. Electroosmotic flows in capillaries or channels that contain the staggered herringbone structure ought to be chaotic and mix adjacent streams efficiently (*20*, *27*). Chaotic flows will also exist in the laminar shear flow in the boundary layer of an extended flow over a surface that presents the staggered herringbone structure. This stirring of the boundary layer should enhance the rates of diffusion-limited reactions at surfaces (e.g., electrode reactions) and heat transfer from solids into bulk flows.

References and Notes

1. M. A. Burns *et al.*, *Science* **282**, 484 (1998).
2. H.-P. Chou, C. Spence, A. Scherer, S. R. Quake, *Proc. Natl. Acad. Sci. U.S.A.* **96**, 11 (1999).
3. D. A. Dunn, I. Feygin, *Drug Discovery Today* **5**, S84 (2000).
4. M. W. Losey, M. A. Schmidt, K. F. Jensen, *Ind. Eng. Chem. Res.* **40**, 2555 (2001).
5. T. S. Sammarco, M. A. Burns, *AIChE J.* **45**, 350 (1999).
6. This condition is based on the following characteristic values: $U < 100$ cm/s, $l \sim 0.01$ cm, $\nu = 0.01$ g/cm·s. For channels, l is typically taken to be the smallest cross-sectional dimension.
7. Poiseuille flows are pressure-driven flows in channels and capillaries. Dispersion refers to the distribution of material by convection in flows in which the velocity is spatially nonuniform. In Poiseuille flows, the speed varies from zero at the walls of the channel to its maximum value in the center. A band of miscible material that spans the cross section of the flow will be dispersed along the direction of the flow as the portions of the band near the center of the channel outpace those near the walls.
8. S. W. Jones, W. R. Young, *J. Fluid Mech.* **280**, 149 (1994).
9. The Péclet number, *Pe*, is a measure of the relative rate of convective transport to diffusive transport in a flow. Mixing becomes more difficult as *Pe* becomes larger. Typical numbers are as follows: $U > 0.1$ cm/s, $l \sim 0.01$ cm, $D < 10^{-5}$ cm^2/s.
10. To estimate the mixing length, we first estimate the time required for diffusion across the channel as l^2/D, then we multiply this time by the average flow speed.
11. S. W. Jones, O. M. Thomas, H. Aref, *J. Fluid Mech.* **209**, 335 (1989).
12. J. M. Ottino, *The Kinematics of Mixing: Stretching, Chaos, and Transport* (Cambridge Univ. Press, Cambridge, 1989).
13. At high Péclet numbers, we estimate the mixing length in a stirred flow by equating the residence time, $\tau_r = \Delta y/U$, and the time for diffusion to act over the reduced width of the unmixed volumes, $\tau_D = \Delta r^2/D = (l^2/D)\exp(-2\Delta y/\lambda)$. We find that $\ln(\Delta y_m/l) + 2\Delta y_m/\lambda \sim \ln(Pe)$, or, for large values of *Pe*, $\Delta y_m \sim \lambda \ln(Pe)$. For flows that are noncha-otically stirred, we expect a power-law dependence of Δy_m on *Pe*.
14. R. H. Liu *et al.*, *J. Microelectromech. Syst.* **9**, 190 (2000).
15. M. Volpert, I. Mezić, C. D. Meinhart, M. Dahleh, Proceedings of the First International Conference on Heat Transfer, Fluid Mechanics, and Thermodynamics, Kruger Park, South Africa, 2001.
16. We made the master structures with two-step photolithography in SU-8 photoresist: The first layer of photolithography defined the channel structure; the second layer defined the pattern of ridges. The pattern of ridges was aligned to lie on top of the channel structure in the first layer. We measured the dimensions of the channel and the ridges using a profilometer. We made molds of the structure in PDMS. To close the channel, we exposed the PDMS to a plasma for 1 min and sealed it to a glass cover slip.
17. J. C. McDonald *et al.*, *Electrophoresis* **21**, 27 (2000).
18. This difference in resistance can be understood as follows: For laminar flows, the height of the channel determines the resistance to flow in the channel, so, in analogy to electronic circuits, flowing over the ridges is like running current through resistors in series (higher total resistance), and flowing along the ridges is like running current through resistors in parallel (lower total resistance).
19. A. Ajdari, preprint *Cond. Mat.* 0101438; *Phys. Rev. E* **65**, 016301 (2002).
20. $\frac{d\Delta\phi}{dy} = \alpha^2 f(q,h,w,\theta)$ with $f(q,h,w,\theta) = \frac{3}{4} qh \left(\frac{4qh - \sinh(2qh) - 2(qh)^2 \coth(qh)}{\sinh^2(qh) - (qh)^2} \right) \sin\theta \cos\theta \frac{\pi}{(h + w)}$. This equation is derived from the ratio of the typical transverse and axial flow speeds in an approximate-model Stokes flow for sinusoidal grooves that is valid for $\alpha \ll 1$ and $w \gg h$. The maximum transverse flow is achieved for $\theta = 45°$ and $\alpha qh \sim 2$. A similar anisotropy is predicted for electroosmotic flows in channels with this geomtery. The details of this calculation will appear elsewhere.
21. Such a sequence of manipulations leads to a baker's transformation of the volumes of fluid that are involved. See (*12*) for a more details.
22. These parameters could equally well be defined with respect to the narrow side of the herringbone structure.
23. We have evaluated the extent of the chaotic region in the cross section by numerically integrating an approximate two-dimensional representation of the transverse flow to generate a Poincaré map. The map is dense (no islands) everywhere in the cross section except in a narrow band (<10% of height) at the top of the channel. We have not systematically optimized the design of the mixer with respect to these $\Delta\phi_m$ and p values.
24. We qualify the mixing as thorough when the fluorescence appears uniform to within the resolution (~2 μm) and sensitivity (down to variations of ~5% of the maximum intensity) of our microscope.
25. R. F. Probstein, *Physicochemical Hydrodynamics* (Butterworths, Boston, 1989).
26. I. Mezić, J. F. Brady, S. Wiggins, *SIAM J. Appl. Math.* **56**, 40 (1996).

27. Recent experimental results confirm that ridges in the floor of a channel do generate transverse components in electroosmotic flows (*28*).
28. T. J. Johnson, D. Ross, L. E. Locascio, *Anal. Chem.* 10.1021/ac010895d.
29. We drove flow in the channels by applying a constant pressure at the inlet reservoir with compressed air. We imaged the evolution of fluorescent streams in the channels using a Leica TCS confocal microscope with a 40×/1.0 numerical aperture objective.
30. Labeled polymers were prepared by allowing poly(ethylenimine) (molecular weight ~500,000) to react with fluorocein isothiocyanate. The product was dialyzed for several days. Diffusivities were calculated based on the broadening of fluorescent streams of the dye in confocal images flows of known speed: $D = 4 \times 10^{-6}$ cm²/s in water and $D = 2 \times 10^{-8}$ cm²/s in 80% glycerol/20% water. Flow speeds were measured by weighing the fluid collected at the outlet of the channel. Viscosity of the glycerol/water solution was estimated to be 0.67 g/cm·s by comparing the flow rate to that of water through the same channel with the same applied pressure.

31. Supported by Defense Advanced Research Projects Agency grants NSF ECS-9729405 and NSF DMR-9809363 Materials Research Science and Engineering Center (A.D.S., S.K.W.D., H.A.S., and G.M.W.); NIH grant GM51559 (A.D.S., S.K.W.D, and G.M.W.); Army Research Office grant DAAG55-97-1-0114 (H.A.S.); and NSF-9875933, NSF DMS-9803555, and a Sloan Foundation Fellowship (I.M.). S.K.W.D. thanks the Deutsche Forschungsgemeinschaft for a research fellowship.

13 September 2001; accepted 14 December 2001

A Group-IV Ferromagnetic Semiconductor: Mn_xGe_{1-x}

Y. D. Park,* A. T. Hanbicki, S. C. Erwin, C. S. Hellberg, J. M. Sullivan, J. E. Mattson,† T. F. Ambrose,‡ A. Wilson,§ G. Spanos, B. T. Jonker‖

We report on the epitaxial growth of a group-IV ferromagnetic semiconductor, Mn_xGe_{1-x}, in which the Curie temperature is found to increase linearly with manganese (Mn) concentration from 25 to 116 kelvin. The *p*-type semiconducting character and hole-mediated exchange permit control of ferromagnetic order through application of a ±0.5-volt gate voltage, a value compatible with present microelectronic technology. Total-energy calculations within density-functional theory show that the magnetically ordered phase arises from a long-range ferromagnetic interaction that dominates a short-range antiferromagnetic interaction. Calculated spin interactions and percolation theory predict transition temperatures larger than measured, consistent with the observed suppression of magnetically active Mn atoms and hole concentration.

Ferromagnetic (FM) semiconductors are materials that simultaneously exhibit semiconducting properties and spontaneous long-range FM order. Classic examples include the europium chalcogenides and the chalcogenide spinels, both extensively studied several decades ago (*1*). The coexistence of these properties in a single material provides fertile ground for fundamental studies (*2*). However, device applications have languished because of low magnetic ordering (Curie) temperatures and the inability to incorporate these materials in thin film form with mainstream semiconductor device materials.

Interest in ferromagnetic semiconductors (FMSs) was rekindled with the discovery of spontaneous FM order in $In_{1-x}Mn_xAs$ in 1989 (*3*) and in $Ga_{1-x}Mn_xAs$ in 1996 (*4*–*6*), when FM properties were realized in semiconductor hosts already widely recognized for semiconductor device applications. These new FMS materials exhibit Curie temperatures up to 35 K and 110 K, respectively, for Mn concentrations of order 5% and sufficiently high hole densities and have been closely studied for their potential in future spin-dependent semiconductor device technologies. For example, $Ga_{1-x}Mn_xAs$ has been used as a source of spin-polarized carriers in both light-emitting diodes (*7*) and resonant tunneling diode heterostructures (*6*, *8*). Electric field control of FM order has recently been reported in $In_{1-x}Mn_xAs$ heterostructures (*9*), demonstrating one of the unique properties of these materials and portending a host of new applications. Experimental evidence for Curie temperatures above 300 K has been reported in other materials, such as $CdMnGeP_2$ (*10*).

We report on the preparation of a group-IV FM semiconductor, Mn_xGe_{1-x}. Although most experimental work on FMS has focused on III-V and II-VI compounds, there is broad interest in the group-IV semiconductors, C, Si, Ge, and $Si_{1-x}Ge_x$. A mean-field solution of a Zener model has recently predicted that FM order can be stabilized in these and other diluted magnetic semiconductor families as well (*11*–*13*). We grew single-crystal Mn_xGe_{1-x}(001) films on both Ge and GaAs(001) substrates. These films have Curie temperatures in the range 25 to 116 K for $0.006 \leq x \leq 0.035$, are *p*-type with carrier densities of $\sim 10^{19}$ to 10^{20} cm^{-3}, and exhibit a pronounced extraordinary Hall effect. Mn_xGe_{1-x} has electronic and magnetic properties that are very promising for FMS device applications. The temperature dependence of the resistivity is semiconducting in character rather than metallic, and the holes mediate the FM exchange, as demonstrated in gated structures where control of the hole density results in corresponding control of FM order at gate voltages compatible with present complementary metal-oxide-semiconductor (CMOS) technology (±0.5 V). In addition, Ge is closely lattice matched to the $Al_yGa_{1-y}As$ family and has higher intrinsic hole mobilities than either GaAs or Si.

A group-IV host may also provide the simplest system for studying the fundamental origins of FM order. To this end, we used density-functional theory to study the electronic structure and magnetic interactions in Mn_xGe_{1-x}, with the aim of providing a first-principles foundation for future model descriptions. We find a strong short-range antiferromagnetic interaction between Mn spins competing with a long-range FM interaction that dominates at all Mn-Mn distances beyond nearest neighbor. From our calculated spin coupling constants and interaction range, we use percolation theory to predict the dependence of the Curie temperature on Mn concentration; the results suggest that a substantial fraction of the Mn does not participate in the FM ordering, consistent with our experimental data.

As with the III-Mn-V FMS compounds, the low solubility of Mn in Ge requires nonequilibrium growth techniques at reduced substrate temperatures to minimize phase separation or the formation of unwanted compounds (*3*–*6*, *14*). The samples were grown by molecular beam epitaxy from elemental Knudsen cell sources at a growth rate of ~5 Å/min. After thermal desorption of the GaAs or Ge(001) substrate surface oxide at ~590°C, a thin buffer layer of Ge was grown at a substrate temperature of 250°C. The substrate temperature was reduced further to 70°C for the growth of Mn_xGe_{1-x} to a typical thickness of 1000 Å to avoid formation of bulk phase precipitates (which plague the III-Mn-V compounds) (*4*, *15*). Reflection high-energy electron diffraction

Naval Research Laboratory, Washington, DC 20375, USA.

*Present address: School of Physics and CSCMR, Seoul National University, Seoul 151-747, Korea.
†Present address: Micron Technology, Boise, ID 33707, USA.
‡Present address: Seagate Technology, Pittsburgh, PA 15203, USA.
§Present address: Boeing Satellite Systems, El Segundo, CA 90009, USA.
‖To whom correspondence should be addressed. E-mail: jonker@nrl.navy.mil